Journal of The Electrochemical Society, **164** (4) A760-A769 (2017)
0013-4651/2017/164(4)/A760/10/$37.00

Solid Phase FePC Catalysts for Increased Stability of Oxygen Reduction Reaction Intermediates at the Cathode/Electrolyte Interface in Lithium Air Batteries

Iromie Gunasekara,[a] Mehmet Nurullah Ates,[a] Sanjeev Mukerjee,[a,*] Edward J. Plichta,[b] Mary A. Hendrickson,[b] and K. M. Abraham[a,*,z]

[a]*Department of Chemistry and Chemical Biology, Northeastern University, Boston, Massachusetts 02115, USA*
[b]*Power Division, US Army RDECOM CERDEC CP&I, RDER-CCP, Aberdeen Proving Ground, Maryland 21005, USA*

Solid-phase catalysts prepared by pyrolysis of Iron(II) phthalocyanine (FePC) embedded in high-surface carbons were evaluated for the catalysis of oxygen reduction reaction (ORR) and oxygen evolution reaction (OER) in Li^+-conducting non-aqueous electrolytes. The ORR mechanism in high donor number (DN) dimethyl sulfoxide (DMSO)-based electrolytes is markedly different from that occurs in low DN acetonitrile(MeCN)-based electrolytes. The ORR is catalyzed by the reduced Fe(I) state of Fe(II)PC. Consequently, the Fe(II)PC/Fe(I)PC redox potential relative to O_2 reduction potential in each electrolyte is important for ORR catalysis. In MeCN-based electrolytes, the Fe(I)PC catalyst is formed at a higher potential than the ORR potential. Hence the catalyzed ORR occurs at the inner-Helmholtz plane of the electrode, stabilizing the superoxide ion (O_2^-) formed by one-electron reduction of O_2, as Fe(I)PC–O_2^-. Indeed, LiO_2 was identified in the Raman spectra of cathodes from discharged Li-O_2 battery cells. In DMSO-based electrolytes, the Fe(I)PC formation potential occurs below the ORR potential and accordingly LiO_2 is more stable in its solvated state in the electrolyte solution as the $Li(DMSO)_n$–O_2^- ion pair. This drives the ORR at the outer-Helmholtz plane of both catalyzed and uncatalyzed electrodes in DMSO-based electrolytes. The FePC embedded carbon electrode doubled the cycle life of Li-O_2 cells utilizing low DN electrolytes.
 [DOI: 10.1149/2.1221704jes]

Manuscript submitted November 21, 2016; revised manuscript received January 24, 2017. Published February 17, 2017.

The limited rechargeability of the Li anode, kinetic limitations of the oxygen electrode reactions and the constraints associated with the development of suitable battery architecture are deterrents to the development of a practical rechargeable Li-O_2 battery.[1] The major discharge product identified in a non-aqueous Li-O_2 battery is Li_2O_2 involving an overall two-electron O_2 reduction which yields a theoretical specific energy of 3505 Wh/kg. This is thirty three percent lower than the theoretical specific energy of 5200 Wh/kg calculated on the basis of the four-electron reduction of O_2 to form Li_2O as the discharge product. Therefore, a cathode catalyst that could catalyze the reduction of O_2 to form Li_2O as the discharge product is appealing.[2–4] Simultaneously, if the same catalyst can promote oxygen evolution reactions at lower over-potentials, then the high capacity of the Li-O_2 battery could be accessed more efficiently in many charge/discharge cycles to realize the goal of an ultra-high energy density rechargeable Li-O_2 battery.

Oxygen electrocatalysts based on transition metal-N_4 centers such as metal porphyrins and phthalocyanines have demonstrated varying degrees of activity to catalyze ORR in batteries and fuel cells.[2,3,5,6] The phthalocyanine macrocycle in particular is a strong electron acceptor which facilitates the axial coordination of the metal center in metal phthalocyanines (MPC) with ligands having a range of electron donor characteristics.[7] Only a few studies have reported ORR/OER catalysis of the O_2 electrode by these metal-N_4 centers in non-aqueous electrolyte-based Li-O_2 batteries.[6,8–10] In this paper we provide evidence for the tunability of the redox potential of the iron(II) phthalocyanine by changing the electron donor property of the ligating solvent molecule. Our results demonstrate the tunability of the ORR catalysis on the metal-N_4 center with respect to the electron donor property of the organic electrolyte (via the solvates, $Li^+(solvent)_n$, formed between the organic solvent and Li^+). We also show that iron(II) phthalocyanine can be transformed into insoluble solid catalysts by appropriate high temperature processing making them potentially useful for practical Li-air batteries. Recent study by Trahan et al. have shown that CoPC-based catalysts influence O_2 electrochemistry in Li-O_2 batteries.[2] According to these authors O_2 reduction reaction mechanism at the catalyst is determined by the solvent's ability to modulate the Lewis acidity of Li^+ in the Li^+-conducting electrolyte solution. In high DN solvents the ORR on the electrode proceeds at the outer-Helmholtz plane since the $Li(solvent)_n^+$–O_2^- intermediate is stabilized in the electrolyte solution. On the other hand, in low DN solvents such as acetonitrile and TEGDME the ORR proceeds at the electrode's inner-Helmholtz plane on the catalyst center since the electron acceptor property of the catalyst is higher than that of the solvated Li^+, $Li(solvent)_n^+$.

An ideal catalyst would be one that selectively catalyzes the ORR and OER reactions without interfering with the performance of the electrolyte or the lithium anode. We demonstrate that the solid phase FePC catalyst that we have developed approach this performance. Our results contrast the data reported by Sun et al.[11] who employed FePC, dissolved in TEGDME and DMSO-based electrolytes, as a redox shuttle for electrons and superoxide ions (O_2^-, the one- electron reduction product of O_2), between carbon cathode and the insulating Li_2O_2 formed on it during discharge. They concluded that the O_2 adsorbed to the FePC present in the electrolyte solution as FePC–O_2 would undergo reduction to form FePC–LiOOLi which would then diffuse to a nucleated Li_2O_2 site and precipitate there. Similarly, they claim that the Fe(III)PC in solution can oxidize the Li_2O_2 to form FePC–O_2^- which would then diffuse to the carbon surface where the superoxide would be oxidized to O_2. However, there was little unambiguous electrochemical or spectroscopic evidence presented to support their solution catalyzed ORR and OER mechanisms. It is important to note that FePC dissolved in the electrolyte solution is an impractical catalyst since it reacts with the Li metal anode and deleteriously affects the rechargeability of the Li-air battery. Consequently, an FePC catalyst that does not dissolve in non-aqueous electrolytes while retaining its ORR and OER catalytic activity would be of great interest for use in Li-air batteries. We have developed such insoluble solid phase catalysts by heat-treating intimate mixtures of high surface area carbon and FePC at selected high temperatures. The properties of these catalysts we have prepared are reported together with their ORR and OER activities in non-aqueous electrolytes and Li-air battery cells. We present a comprehensive discussion of the structure-catalytic property relationships of these novel solid phase FePC embedded in carbon cathodes and the manner in which the non-aqueous electrolytes influence their electrochemical activity. The FePC embedded carbon cathodes have doubled the cycle life of Li-air battery cells.

*Electrochemical Society Fellow.
[z]E-mail: kmabraham@comcast.net

Experimental

Materials.—The battery grade lithium salts ($LiPF_6$, $LiCF_3SO_3$), Iron (II) phthalocyanine and dry organic solvents (acetonitrile- MeCN, dimethyl sulfoxide- DMSO) were purchased from Sigma-Aldrich and were stored in an Ar-filled MBraun glove-box maintained under 0.5 ppm H_2O prior to use. The high surface area carbons, Vulcan-XC72R (233 m^2/gram) and Ketjenblack-EC300JD (802 m^2/gram), were obtained from Cabot corporation. The $Ag/AgNO_3$ reference electrode was prepared as reported by Wain et al.[12] using a silver wire (99%) purchased from Alfa Aesar. All the potentials presented in this paper are reported with respect to the Li/Li^+ reference electrode unless otherwise stated.

Iron(II) phthalocyanine–based catalyst synthesis.—Catalysts were prepared using a method previously reported by Dodelet et al.[3,13] Iron(II) phthalocyanine dissolved in concentrated sulfuric acid was stirred with the carbon black (Ketjenblack-EC300JD or Vulcan-XC72R). The amount of high surface area carbon added was such that the weight of iron metal in the final carbon-catalyst matrix is 4% by weight. The resulting slurry was poured into a large volume of de-ionized water cooled down to below 5°C. The suspension was filtered and washed as required to remove any residual H^+ in the catalyst. The carbon-catalyst residue was dried overnight at 60°C under vacuum and the dried powder was heat treated at the selected temperatures (presented in the Results and discussion section) for two hours under argon gas.

Cyclic voltammetry.—Thin film electrodes were prepared from FePC/Vulcan catalyst inks as follows. PVDF binder was dissolved in N-methyl-2-pyrrolidone to which the carbon/catalyst powder was added so that the binder:(carbon/catalyst) ratio was 10:90 by mass. A required aliquot of the ink dispersion was deposited on the clean dry glassy carbon disk electrode surface to obtain a 0.1 mg cm^{-2} catalyst layer. The glassy carbon disk was dried in vacuum at 80°C overnight.

Voltammograms were initially recorded in Ar saturated 0.1 M $LiCF_3SO_3$/MeCN, 0.1 M $LiPF_6$/MeCN, 0.1 M $LiCF_3SO_3$/DMSO, and 0.1 M $LiPF_6$/DMSO electrolytes to investigate the redox activity of the catalyst metal center and to verify the absence of electrochemical reactions that arise from the electrolyte within the electrochemical potential window of interest. All the electrochemical data shown in this paper were obtained at a glassy carbon disk electrode (0.5 cm diameter) and the current densities reported here are referenced to its geometric surface area (0.196 cm^2). Oxygen electrochemistry was recorded in O_2 saturated 0.1 M $LiCF_3SO_3$ or $LiPF_6$ electrolytes prepared in MeCN and DMSO solvents.

Fourier transform infrared spectroscopy (FT-IR).—Commercial Iron(II) Phthalocyanine samples pyrolyzed at different temperatures under argon were analyzed using a Bruker Vertex-70 FT-IR spectrometer.

In-situ raman spectroscopy.—In-situ Raman experiments were carried out using an in-situ Raman cell obtained from MTI Corporation. $Li-O_2$ cells for these studies were prepared using a carbon cloth cathode (facing the quartz window of the Raman cell) and a lithium anode. Raman spectra were obtained in a DMSO-based electrolyte containing dissolved FePC of the composition 1 mM FePC/0.1 M $LiCF_3SO_3$/DMSO. The spectra were recorded after scanning the cathode potential in 200 mV steps from open circuit and holding the electrode at each potential for more than 300 minutes. Note that whereas unheated FePC is soluble in DMSO, the heat-treated FePC/carbon materials are insoluble in this solvent.

Transmission electron microscopy (TEM).—The Iron(II) Phthalocyanine/carbon catalysts were characterized using a JEOL 2010F transmission electron microscope.

$Li-O_2$ cells.—Li-oxygen cells were constructed using Li foil anodes and uncatalyzed cathodes using Ketjenblack EC300JD, and catalyzed carbon cathodes containing FePC/Ketjenblack-based catalyst. The two electrodes were separated by means of microporous polypropylene membrane separators. Details of our $Li-O_2$ cell construction are reported elsewhere.[14] The $Li-O_2$ cells employed 1 M $LiPF_6$/TEGDME or 1 M $LiCF_3SO_3$/TEGDME electrolytes. Some cycled cells were disassembled and the cathodes were analyzed by means of several spectroscopic techniques that are discussed later in this paper.

All electrochemical experiments and $Li-O_2$ cell tests were carried out in a glove-box maintained at a humidity level < 0.5 ppm.

X-ray diffraction.—X-ray diffraction spectra of the FePC/Carbon catalysts were recorded using a Rigaku Ultima IV diffractometer using a Cu Kα radiation source.

Discharged $Li-O_2$ cells were disassembled inside the glove-box, the carbon cathodes were separated, washed with acetonitrile to remove the Li salt, and XRD spectra were recorded with a Rigaku Ultima IV diffractometer using a Cu K_α radiation source. (The cathode sample was covered with a Kapton polyimide film to prevent contact with atmospheric moisture during the data acquisition).

Results and Discussion

Electrochemistry of iron(II) phthalocyanine dissolved in dimethyl sulfoxide.—Iron(II) phthalocyanine (FePC) having the molecular structure (I) is soluble in dimethyl sulfoxide (DMSO) and its Li salt solutions. We have prepared insoluble materials which retain the $Fe-N_4$ framework and the ability to catalyze O_2 reduction and evolution reactions, by heat-treating FePC embedded in high surface area carbons, at selected high temperatures. The solubility of FePC in DMSO has allowed us perform an in-depth study of its electrochemistry first and compare with that of the solid phase carbon/FePC materials. We have performed these studies in electrolytes prepared in the high electron donor solvent, dimethyl sulfoxide ($(CH_3)_2SO$, DMSO) and the low electron donor solvents, acetonitrile (CH_3CN, MeCN) and tetraethylene glycol dimethyl ether ($CH_3O(C_2H_4O)_4CH_3$, TEGDME). Their Gutmann Donor Numbers (DN), which are measures of the solvent's electron donating ability, are, DMSO, 29.8, MeCN, 14.1 and TEGDME, 16.6. The higher the solvent's DN, the greater is its electron donating ability (Lewis basicity) to form a complex with an electron acceptor (Lewis acid) like Li^+.

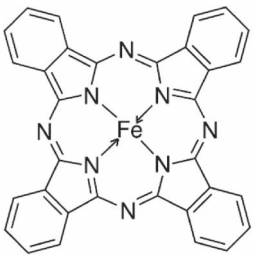

(I)

Iron(II) Phthalocyanine

Cyclic voltammograms recorded on a glassy carbon (GC) electrode in Ar saturated 1 mM FePC solutions in 0.1 M $LiCF_3SO_3$/DMSO and 0.1 M $LiPF_6$/DMSO electrolytes are shown in Figure 1. Three pairs of redox reactions are observed. The Fe(II)/Fe(I) reversible reaction with a reduction peak at 2.62 V is consistent with the changes observed in the in-situ Raman spectrum at this potential (Figure 2). While all the peaks in the Raman spectrum obtained at open circuit potential (3.02 V) are due to the DMSO solvent, new Raman peaks appear at 260, 584, 745, 1000 cm^{-1}, and between 1100–1500 cm^{-1} when the electrode potential is scanned to slightly below the 2.62 V peak. It is important to review the electronic configuration of Fe presented in

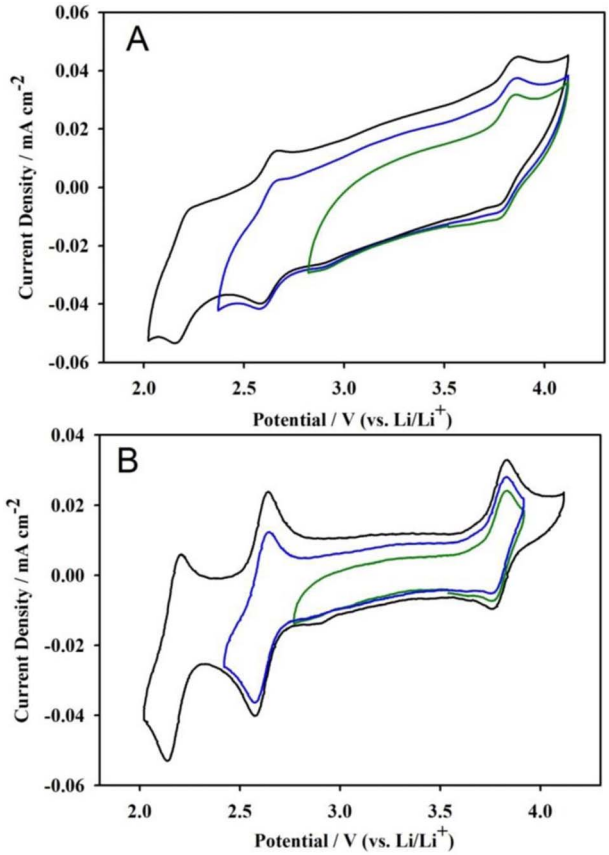

Figure 1. Cyclic voltammograms recorded on a glassy carbon electrode in argon purged 1 mM solution of FePC in A) 0.1 M $LiPF_6$/DMSO and B) 0.1 M $LiCF_3SO_3$/DMSO. Scan rate is 10 mV s^{-1}. The potentials are indicated versus a Li/Li^+ reference electrode. CVs depicted in different colors in each represent current-voltage scans recorded at different potential windows.

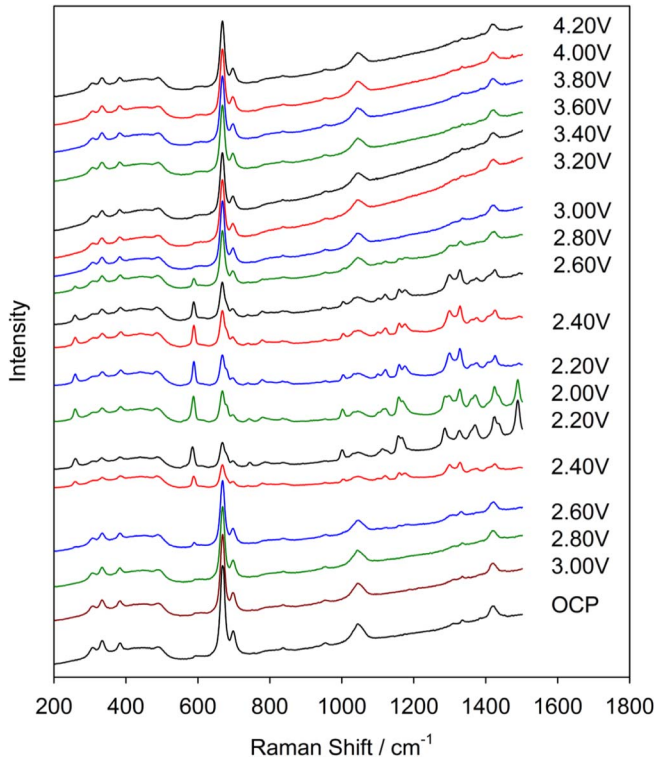

Figure 2. In-situ Raman spectra obtained at the carbon electrode at different potentials versus Li/Li^+ in argon purged 1 mM FePC dissolved in 0.1 M $LiCF_3SO_3$/DMSO.

Scheme 1 as a function of its oxidation state to understand these Raman spectra since the Fe oxidation state changes during the potential scan.

In solvents such as DMSO which can form coordination bonds with electron acceptor centers, Iron(II) phthalocyanine is six

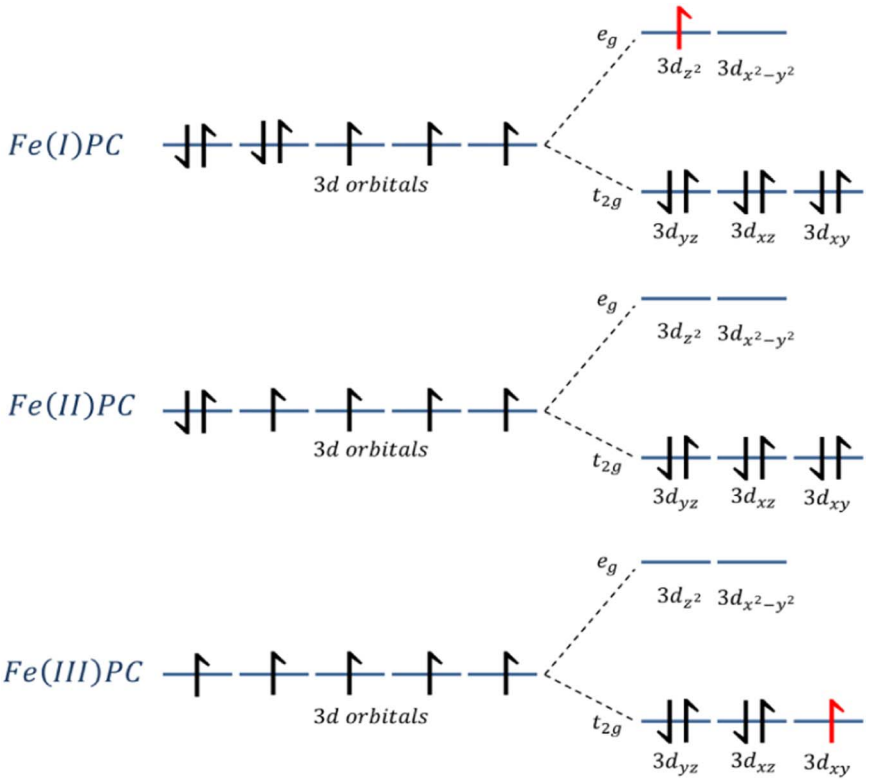

Scheme 1. Iron (Fe) *d* electron configurations of FePC dissolved in DMSO as a function of the oxidation state of iron.

$$(DMSO)_2Fe(II)PC + e^- \leftrightarrow [(DMSO)_2Fe(I)PC]^- \quad [1]$$

$$[(DMSO)_2Fe(I)PC]^- \leftrightarrow [(DMSO)Fe(I)PC]^- + DMSO \quad [2]$$

Scheme 2. Equations 1 and 2 representing Fe(II)/Fe(I) Redox Reactions in DMSO.

$$[(DMSO)Fe(I)PC]^- + e^- \leftrightarrow [(DMSO)Fe(I)PC]^{2-} \quad [3]$$

Scheme 3. Equation 3 representing Fe(I)PC Reduction in DMSO.

coordinated[15,16] in the structure, $(DMSO)_2$Fe(II)PC, containing two DMSO molecules as shown in Scheme 2. At the open circuit potential the metal center in this structure is in the Fe(II) state. When the electrode is polarized to lower potentials, the Fe(II) is reduced to Fe(I) which has the $(xz,yz,xy)^6(z^2)^1$ electronic configuration. If the DN of the coordinating molecule is high as in DMSO, a six coordinated complex having the Fe(I) electronic configuration is unstable and the redox potential of Fe(II)/Fe(I) is shifted downwards[17] (Equation 1) compared with that in a low DN solvent-based electrolyte, eg. $LiPF_6$/TEGDME that does not readily complex with Fe(II)PC. This shift of the Fe(II)/Fe(I) redox potential relative to the nature of the electrolyte is profound and affects the mechanism of O_2 electrochemistry as discussed later in this paper.

As shown in Equation 2 in Scheme 2, the $(DMSO)_2$Fe(I)PC formed by reduction releases one of the two DMSO molecules to form an asymmetric five coordinated complex. The planarity of the $(DMSO)_2$Fe(II)PC molecule is lost during this transition and the changes that appear in the Raman spectra below 2.6 V are consistent with these symmetry changes.

When Fe(I)PC is further reduced as displayed in Figure 1, the electron is acquired by the PC macrocycle (Scheme 3). In this process only the PC macrocycle moiety is reduced. This is reflected by the new Raman peaks that appear at 1425 and 1490 cm^{-1} in Figure 2 when the electrode is polarized down to 2.20 V. These Raman peaks can be attributed to the pyrrole C-C and C-N stretching vibrations arising from the reduction of the macrocycle ring as depicted in the equation of Scheme 3.

The oxidation of Fe(II) to Fe(III) that appears at 3.8 V in the reverse scan (in $LiCF_3SO_3$/DMSO and in $LiPF_6$/DMSO) is a two-step reaction where the electron transfer is followed by substitution of a coordinated DMSO molecule by an anion as depicted in Scheme 4. The strength of the coordination bond between the anion (X^-) in solution and the Fe(III) center determines the redox potential of the Fe(II)/Fe(III) couple. That is, the oxidation of the Fe(II) to Fe(III) occurs at a lower potential if the anion forms a stronger bond with the Fe(III)PC formed from the oxidation.[15,17] This in turn is determined by the electron donor property (DN) of the anion. As we have shown[18,19] before $CF_3SO_3^-$ has a DN of 16.9 as opposed to PF_6^- with a low DN of 2.5.

We have also studied the redox behavior of FePC/Vulcan-based catalysts in argon saturated electrolytes in DMSO and the data obtained, consistent with the preceding results, are discussed later in the section dealing with catalyzed ORR. Overall FePC showed similar redox behavior in acetonitrile-based electrolytes except that the various redox peaks are observed at higher potentials. The solubility of FePC in acetonitrile (MeCN) is much less than in DMSO and, as a result, we used a saturated solution of FePC in MeCN-based electrolytes

$$(DMSO)_2Fe(II)PC \leftrightarrow [(DMSO)_2Fe(III)PC]^+ + e^- \quad [4]$$

$$[(DMSO)_2Fe(III)PC]^+ + X^- \leftrightarrow (DMSO)Fe(III)PCX + DMSO \quad [5]$$

Scheme 4. Equations 4 and 5 representing Fe(II)/Fe(III) oxidation reaction in DMSO.

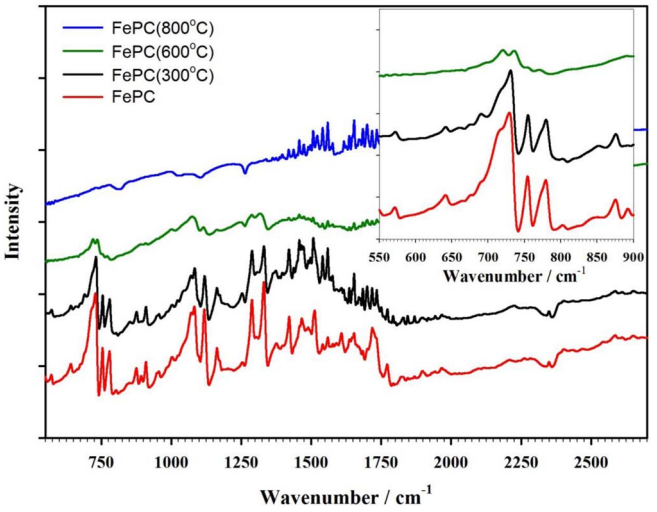

Figure 3. FT-IR spectra of pure Iron(II) phthalocyanine pyrolyzed at a series of temperatures ranging from 300–800°C. Inset of the graph shows the expanded region of the spectrum from 550 cm^{-1} to 900 cm^{-1}.

to study FePC electrochemistry. Potential shifts attributed to solvent DN on ORR catalysis is discussed later in conjunction with catalyzed ORR in MeCN-based electrolytes.

Thermal stability and structure of iron(II) phthalocyanine.—FT-IR spectra recorded to analyze neat FePC and FePC samples heated at 300°C, 600°C and 800°C under argon gas are presented in Figure 3. The IR peaks centered at 730 cm^{-1} arise from the out-of-plane C-H vibrations characteristic of the α and β polymorphic forms of FePC.[20] Both FePC and FePC (300°C) show marked similarity in the IR spectra in this region. The unheated FePC is in the α polymorphic form which for our sample is confirmed by the FT-IR peak observed at 728 cm^{-1}, and there is no change in the polymorphism at 300°C (Figure 4). The α-FePC is transformed to the β form upon further heating. At 600°C, the FePC is completely converted to the β polymorph, as indicated by the IR peak at about 740 cm^{-1}.

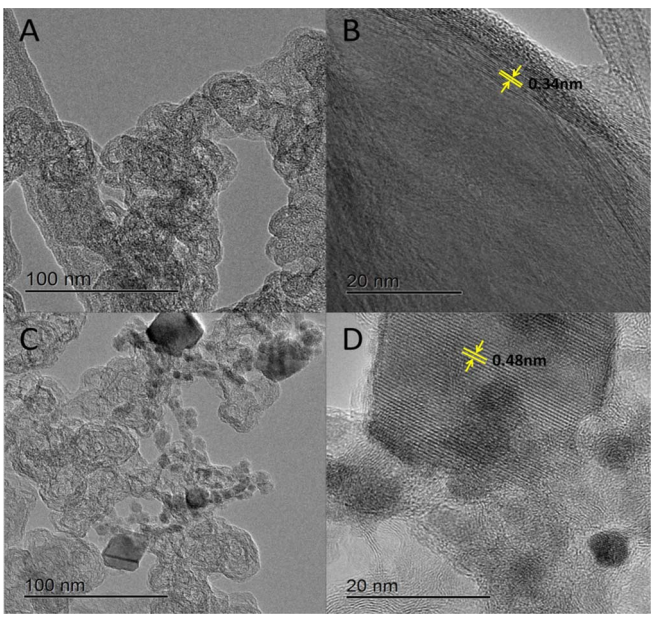

Figure 4. TEM micrographs of catalysts, A, B) FePC/KB(300), C, D) FePC/KB(600) showing their crystalline nature.

The FT-IR spectrum for the FePC (600°C) material has peaks at 1080 cm^{-1}, 1120 cm^{-1} and 1331 cm^{-1} which can be attributed to C-N stretching, C-H bending (in-plane) and pyrrole stretching (C=C or C=N), respectively.[21] This observation supports the notion that the M-N_4 macrocycle is still intact after the heat-treatment at 600°C.[21] Meanwhile the FT-IR peak at 730 cm^{-1} present in the α form shifts to 740 cm^{-1} at 600°C. This latter peak is indicative of the β polymorphic form. Therefore, we can conclude that at 600°C the FePC is substantially converted to the β polymorph, with its partial decomposition (breakdown of the benzene rings)[20,22,23] also possibly occurring. However, Fe-N_4 moiety appears to be retained in the resulting FePC (600°C) material. The FePC sample pyrolyzed at 800°C showed complete absence of the IR peaks that arise from the C-N macrocycle suggesting the destruction of the M-N_4 center.

Synthesis and characterization of carbon supported catalysts.— Carbon supported FePC electrode materials were prepared using two types of carbon precursors, low surface area Vulcan-XC72R (VC) and high surface area Ketjenblack-EC300JD (KB). The FePC/Vulcan-XC72R (VC)-based catalysts were synthesized to carry out electrochemical thin film studies, and the FePC/Ketjenblack-EC300JD (KB)-based catalysts were prepared to evaluate Li-O_2 cell performance. In the following sections the Vulcan and Ketjenblack supported catalysts prepared at 300°C will be referred to as FePC/VC(300) and FePC/KB(300), respectively. The carbon/FePC electrode materials prepared at other temperatures will be named in the same manner with the corresponding temperature identifiers.

The powder X-ray diffraction (XRD) spectra of the FePC/Carbon-based catalysts prepared by heat-treatment indicated the formation of metallic Fe ($2\theta = 44°$) in the sample pyrolyzed at 800°C. The FePC/carbon samples prepared at 300°C and 600°C showed little change in their XRD. This is in agreement with the FT-IR spectra which as mentioned above showed that the 300°C and 600°C samples retained the Fe-N_4 center while complete destruction of the phthalocyanine macrocycle occurred at 800°C. Therefore, the rest of the investigations were focused on the catalysts prepared at 300°C and 600°C.

Transmission electron microscopic images obtained for the catalysts prepared at 300°C and 600°C are shown in Figure 4. The distance of 0.48 nm between the lattice planes for the crystalline regions in FePC/KB(600) shown in Figure 4D is consistent with the FePC being in the β polymorphic form.[20] Meanwhile the FePC/KB(300) catalyst showed a distance of 0.34 nm between the lattice planes which is similar to the Fe-Fe distance observed for FePC in the α polymorphic form.[20] These results are in agreement with the IR spectra presented earlier. It appears that the FePC embedded in the carbon is more stable under heat-treatment than pure FePC. As a result, the catalyst adsorbed on carbon does not undergo significant decomposition at 600°C but remains in the carbon matrix substantially as the β polymorph.

The solubility of the carbon supported FePC/(300) and FePC/(600) catalysts in TEGDME were tested by stirring 1 mg of the catalyst in 1 ml of TEGDME. The FT-IR spectra and visual examination of the color of supernatant solutions obtained for each catalyst, compared to the neat TEGDME solvent and a solution of 1 mM FePC/TEGDME, indicated that all of the catalysts were insoluble in TEGDME. The catalysts remained strongly adsorbed to the solid carbon matrix for the observed period of more than a month. We have performed a detailed study of the catalyst solubility in TEGDME because we expect this solvent to be used in practical Li-air batteries.

Oxygen reduction reactions in high DN dimethyl sulfoxide-based electrolytes.—Figure 5 shows the cyclic voltammograms obtained for an O_2 saturated solution in $LiPF_6$/DMSO at a glassy carbon electrode containing thin films of two FePC/VC-based catalysts. The same onset potentials on the catalyzed and glassy carbon electrodes suggest that the FePC/VC catalysts do not influence the ORR in DMSO. While the Fe(II)/Fe(I) redox potential appears at 2.62 V (Figure 1), the onset of the O_2 reduction reaction is seen at about 2.9 V. The pre-peak which starts to form at 3.3 V the O_2 saturated electrolyte can be attributed to

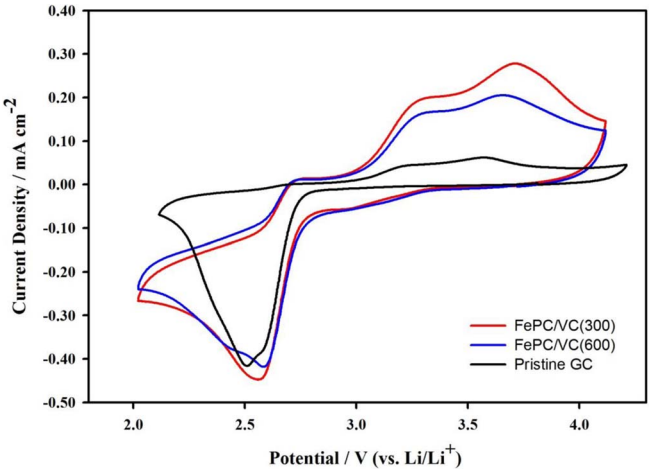

Figure 5. Cyclic voltammograms obtained at a glassy carbon disk, with and without catalysts, in O_2 saturated 0.1 M $LiPF_6$/DMSO. Scan rate is 10 mV s^{-1}.

adsorption of O_2 on the metal center of the catalyst. Comparison with the data in Figure 1 indicates that the iron remains in the Fe(II) state at the superoxide forming potential of 2.9 V (i.e, the onset potential of ORR) in DMSO. The Fe(II)PC would not stabilize the superoxide formed as stabilization would occur only by pairing the unpaired electron in O_2^- with the e_g^1 electron in Fe(I)PC which starts to form at 2.7 V. Consequently, the superoxide ion is more stable in the DMSO electrolyte solution as the $Li^+(DMSO)_n$–O_2^- ion pair.[2,24]

The first of the two closely lying reduction peaks in the CV in Figure 5 at about 2.5 V peak is attributed to the formation of the $Li^+(DMSO)_n$–O_2^- ion pair and the second to its reduction to Li_2O_2 as we reported before for ORR in DMSO-based electrolytes.[24] The present results are reminiscent of the previously discussed O_2 reduction on the CoPC catalyst in DMSO-based electrolytes involving an outer Helmholtz plane electron transfer mechanism.[2] Thus, ORR on both FePC and CoPC catalysts in DMSO-based electrolytes are outer-Helmholtz plane reactions.

Oxygen reduction reactions in low DN acetonitrile-based electrolytes.—Two requirements must be fulfilled for catalytic ORR at the inner Helmholtz plane of the electrode: i) the stabilization of the superoxide ion on the metal center, which is determined by the presence of Fe(I)PC with the e_g^1 electronic configuration of the Fe(I) state (Scheme 1), and ii) lower stability of the superoxide ion in the electrolyte solution than on the metal center which is a function of the electrolyte solvent's DN. Electrochemical data we currently have suggest that an electrolyte in a low DN solvent, with DN less than about 20, would facilitate ORR on the metal center involving an inner-Helmholtz plane electron transfer.[2] Our ORR data presented below for electrolytes in acetonitrile (DN = 14.1) support this view.

FePC is only sparingly soluble in MeCN. Therefore, saturated solutions containing < 0.5 mM FePC were used to determine the redox behavior of neat FePC in MeCN electrolytes. Cyclic voltammograms of FePC/VC(300) thin films (on GC electrode) recorded in Ar saturated solutions of 0.1 M $LiCF_3SO_3$/MeCN are shown in Figure 6A. The reduction peak observed at around 3.2 V in Figure 6A is consistent with that expected for the Fe(II) → Fe(I) transition. The corresponding reverse reaction peak appears at 3.4 V in the oxidation wave. The pair of redox peaks that appear around 3.8 V is most probably due to the Fe(II)/Fe(III) oxidation/reduction processes. As we have shown before,[24,25] the life time of the initially formed O_2^- on uncatalyzed electrodes is too short to be detected electrochemically. The Fe(II)/F(I) redox reactions at ~3.2 V in both the dissolved FePC and in the Fe(II)PC/carbon solid catalysts occur about 300 mV above the O_2 reduction onset at 2.9 V. The 3d eg^1 electronic configuration in the Fe(I)PC catalyst (see Scheme 1) obtained at 3.2 V from the reduction

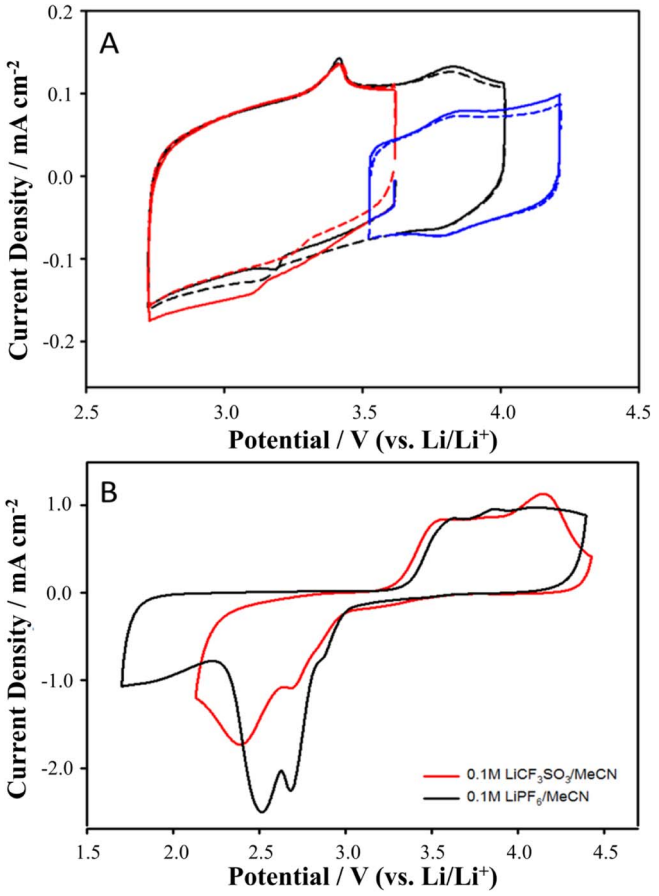

Figure 6. Cyclic voltammograms obtained on a FePC/VC(300) electrode in: A) an Ar saturated solution of 0.1 M $LiCF_3SO_3$/MeCN (Solid line-first cycle, dotted line-second cycle); the three different color CVs are current-potential scans at different potential ranges; B) O_2 saturated solutions of 0.1 M $LiCF_3SO_3$/MeCN (red) and $LiPF_6$/MeCN (black).

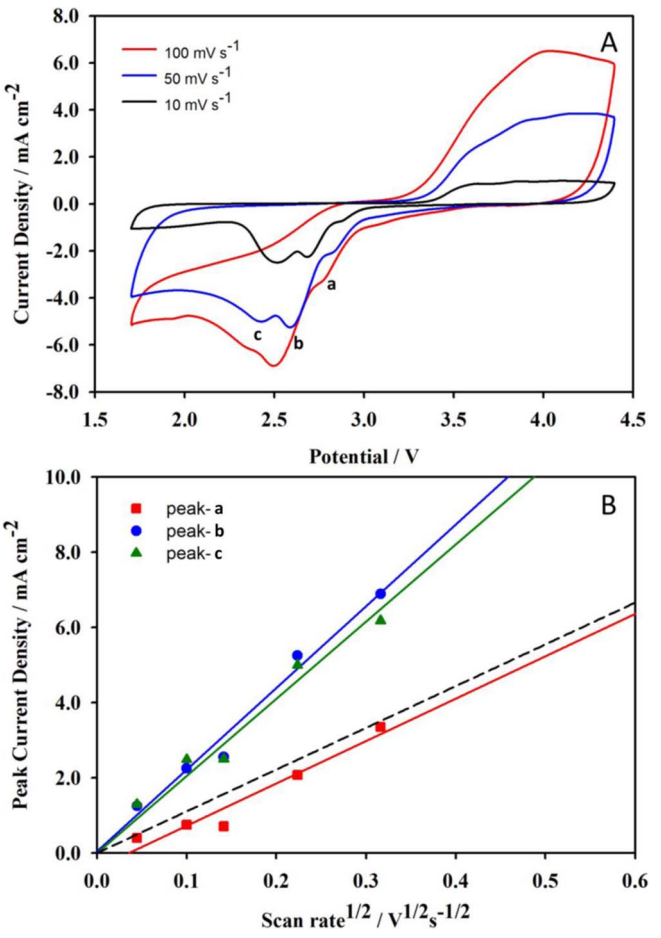

Figure 7. A) Cyclic voltammograms obtained for FePC/VC(300) in oxygen saturated solutions of 0.1 M $LiPF_6$/MeCN at scan rates ranging from 10–100 mV s^{-1}, B) Nicholson-Shain plots for the ORR peak currents obtained at FePC/VC(300). (The dotted line indicates the theoretical Nicholson-Shain plot for n = 1.)

of Fe(II)PC present at the inner-Helmholtz plane of the electrode is able to stabilize the superoxide ion formed by one-electron reduction of O_2.

Comparison of the cyclic voltammograms obtained in O_2 saturated solutions of 0.1 M $LiPF_6$/MeCN and 0.1 M $LiCF_3SO_3$/MeCN suggest that there are three consecutive electron transfer processes at the FePC/VC(300) electrode during the reduction cycle (Figure 6B). We also found that in spite of the change in polymorphism of FePC, the redox activity of the FePC/VC(600) is preserved as revealed by the redox behavior of FePC/VC(600) in argon saturated 0.1 M $LiCF_3SO_3$/MeCN.

Figure 7 displays the cyclic voltammograms recorded in O_2 saturated solutions of 0.1 M $LiPF_6$ in MeCN on the FePC/VC(300) electrode at different potential scan rates. Besides the pre-peak due to O_2 adsorption, there are three distinct reduction peaks that appear at 2.9 V, 2.7 V and 2.5 V. Nicholson-Shain plots derived from the peak currents in Figure 7A are shown in Figure 7B. The number of electrons involved in each reaction was calculated using the Nicholson-Shain equation (Equation 6) where i_{pc} is the peak current density; n is the number of electrons, α is the transfer coefficient taken as 0.5, D_o is the O_2 diffusion coefficient, C_o is the oxygen concentration and ν is the scan rate.

$$i_{pc} = \left(2.99 \times 10^5\right) n(n\alpha)^{1/2} D_o^{1/2} C_o \nu^{1/2} \quad [6]$$

The calculated Nicholson-Shain plot for one-electron reduction of oxygen in MeCN is shown as a dotted line in Figure 7B. The plot calculated for the first reduction peak (a) is in good agreement with the theoretical plot for one-electron reduction of O_2. Meanwhile, the slope of the plots obtained for the second (b) and third (c) reduction peaks are almost twice as that the first reduction. Therefore, it appears as if peak (a) represents a one-electron reduction of O_2 while peaks (b) and (c) represent two-electron reduction reactions. If the two-electron reduction process involves O_2 reduction intermediate sitting on the catalytic site as the reactant, this process cannot be represented by the Nicholson-Shain equation that is relevant to dissolved species. Therefore, we conclude that peaks (b) and (c) represent direct reduction of oxygen to Li_2O_2 at two different sites at the inner-Helmholtz plane on the electrode. The second reduction peak (b) probably corresponds to the two-electron reduction of O_2 to Li_2O_2 on the Fe(I)PC catalyst and peak (c), at least partially, to Li_2O_2 formed at a second type of catalyzed or uncatalyzed sites on the electrode. The current density of peak (c) supports the argument that the reduction of the Li_2O_2 to Li_2O also is probably occurring at this wide potential region.

Figure 8 summarizes the electrochemical responses obtained for the catalyzed electrodes (FePC/VC(300) and FePC/VC(600)) in O_2 saturated solutions. The cyclic voltammograms obtained at both FePC/VC(300) and FePC/VC(600) catalyzed electrodes show the peak at 2.9 V most probably due to the formation of the FePC stabilized O_2^- (FePC–O_2^-). Interestingly, the ORR peak at 2.7 V prominent on the FePC/VC(300) catalyzed electrode (discussed above) is very weak or non-existent on the FePC/VC(600) electrode. This suggests that the two-electron reduction of O_2 to Li_2O_2 is dominant reaction on this catalyzed electrode. The (FePC–O_2^-) stabilized at the catalysts surfaces at about 2.9 V would combine with Li^+ and undergo

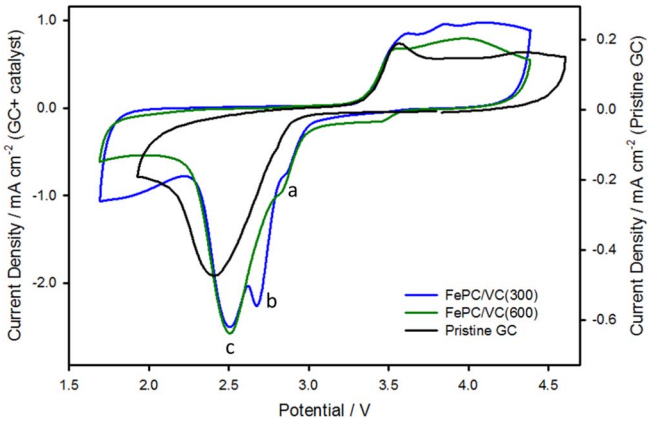

Figure 8. Cyclic voltammograms of O_2 saturated solutions of 0.1 M $LiPF_6$/MeCN on FePC/VC electrodes. Scan rate is 10 mVs^{-1}.

chemical decomposition to Li_2O_2 as discussed below in the mechanistic section.

Mechanistic considerations of FePC catalysis.—The reactions that most probably take place on the FePC/VC(300) catalyst during ORR are shown in Equations 7–9 of Scheme 5 and Figure 9. Molecular oxygen that is adsorbed on the iron center is reduced to superoxide which is stabilized on the catalytic sites, as shown in Reaction 7. The second reaction involves the formation of Li_2O_2 via chemical interaction and decomposition of the superoxide residing in two nearby catalytic sites (Equation 8). Therefore, we can conclude

Reduction pathway (i)

$$N_4Fe + O_2 + e^- + Li^+ \rightarrow N_4Fe - O_2Li \quad [7]$$

$$2N_4Fe - O_2Li \rightarrow N_4Fe - O_2Li_2 + O_2 \quad [8]$$

$$N_4Fe - O_2Li_2 + 2Li^+ + 2e^- \rightarrow 2Li_2O + N_4Fe \quad [9]$$

Reduction pathway (ii)

$$N_4Fe + O_2 + 2e^- + 2Li^+ \rightarrow N_4Fe - O_2Li_2 \quad [10]$$

Reduction pathway (iii)

$$2N_4Fe + O_2 \rightarrow N_4Fe - O - O - FeN_4 \quad [11]$$

$$N_4Fe - O - O - FeN_4 + 2e^- + 2Li^+ \rightarrow N_4Fe - O_2Li_2 - FeN_4 \quad [12]$$

Oxidation

$$2N_4Fe - Li_2O \rightarrow N_4Fe - Li_2O_2 - FeN_4 + 2Li^+ + 2e^- \quad [13]$$

$$N_4Fe - Li_2O_2 - FeN_4 \rightarrow N_4Fe + O_2 + 2Li^+ + 2e^- \quad [14]$$

$$N_4Fe - LiO_2 \rightarrow N_4Fe + O_2 + Li^+ + e^- \quad [15]$$

Scheme 5. Equations 7–15 representing proposed mechanisms of the catalytic oxygen reduction and oxygen evolution reactions at FePC/VC(300) under CV conditions.

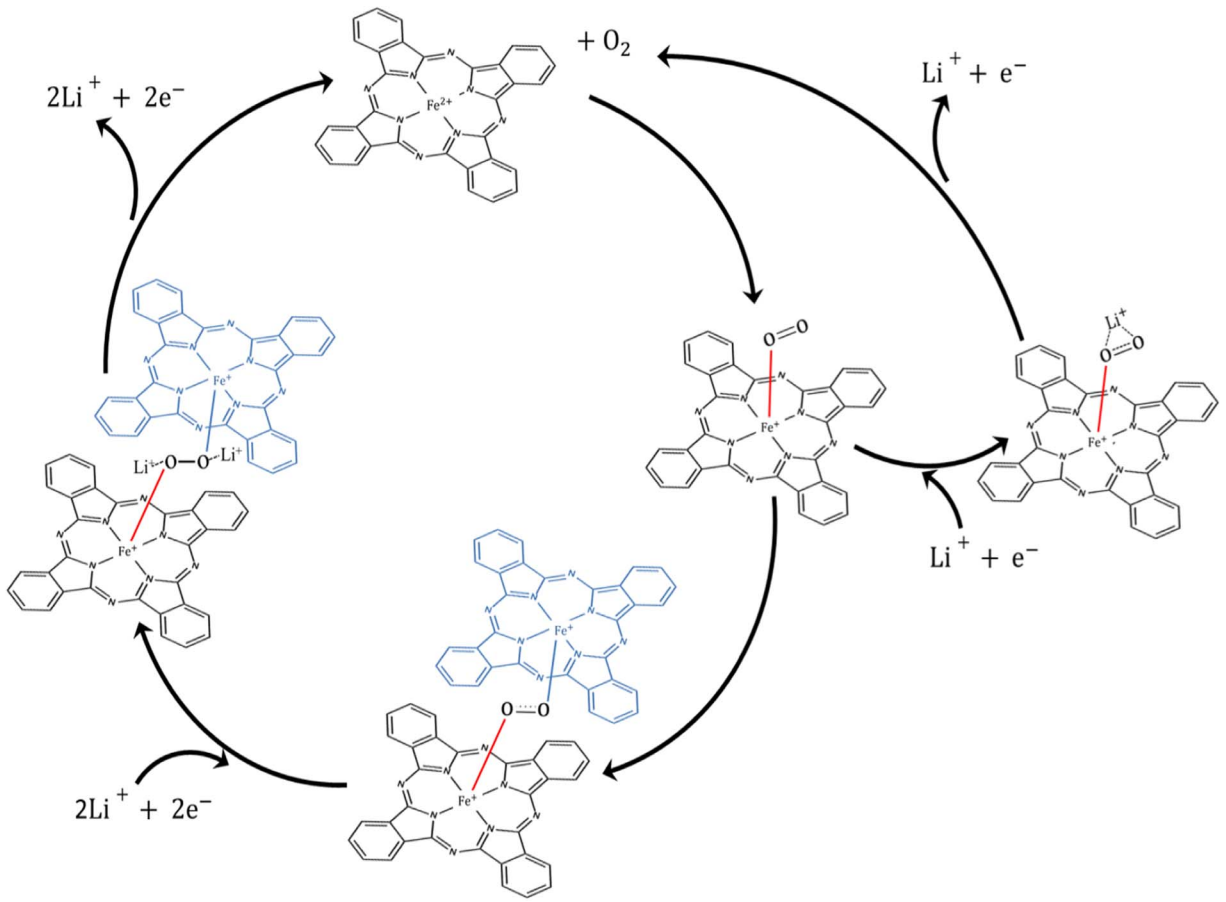

Figure 9. Pathway (i and iii) - Proposed mechanism of the catalysis of oxygen reduction and oxygen evolution reactions at the FePC/VC(300) catalyst.

that the changes in crystallinity of the FePC phase due to the reduction of the Fe metal center is muted in the carbon supported catalyst. Direct two-electron reduction of oxygen to lithium peroxide would also take place on some catalytic sites (Equation 10) as the electrode is scanned to lower potentials.

Equations 13–15 show the possible oxidation reactions of the lithium oxides produced from ORR to O_2 at the catalyzed electrodes.

The short Fe-Fe interatomic distance in α-FePC is appropriate to facilitate reactions 8 and 12 in Scheme 5. The longer Fe-Fe distance in the β-polymorphic form present in the FePC/VC(600) catalyst probably does not allow efficient interaction of the superoxide species residing on two adjacent FePC centers and as a result this catalyst may discourage this mode of formation of Li_2O_2. Instead, it would provide a higher degree of stability to the Fe(I)PC–O_2^- intermediate increasing its life time on the electrode. The second reduction peak (peak (b) in Figure 8) observed at the FePC/VC(300) catalyzed electrode can be attributed to the direct two-electron reduction of O_2 to lithium peroxide involving two adjacent catalytic sites (Equation 10–12). The data appear to support the view that both FePC/VC(300) and FePC/VC(600) catalysts efficiently reduce O_2 to Li_2O_2 via two-electron reduction of O_2. As mentioned earlier, some reduction of Li_2O_2 to Li_2O, at least on the FePC/VC(300) catalyst as shown in Equation 9, cannot be ruled out. This is reminiscent of the O_2 reduction reaction we previously observed on CoPC catalyzed electrodes.[2] Electrode passivation by the Li_2O_2 formed on the electrode makes it difficult to unequivocally characterize this process.

For each catalyst current-voltage scans in O_2 saturated solutions were recorded for five consecutive cycles. The magnitude of the peak (a) decreased after each cycle on both FePC/VC(300) and FePC/VC(600) in the CVs recorded in the potential range of 2.8 V and 4.4 V. As the cathodic limit of the current-voltage scan was extended to 1.7 V, peak (a) and (b) disappeared in the second cycle. The underlying reason behind this observation is probably the passivation of the catalyst by the ORR products or the reactions of the ORR intermediates with the FePC macrocycle. When the CV potential is reversed below 1.7 V the excess superoxide ions not bound to the Fe- center have sufficient time to react with the FePC macrocycle and thereby decrease the activity of the catalyst. The catalyst can also be poisoned by the insoluble ORR products deposited on it.

The preceding electrochemical data for FePC/VC(300) and FePC/VC(600) catalysts validate the importance of the metal macrocyclic Fe-N_4 center for the stabilization of the initially formed superoxide. The ORR and OER processes in the FePC embedded electrodes are assisted by the Fe-N_4 center as indicated by the reaction pathways depicted in Figures 9 and 10. The two pathways depict the two ORR routes predicted by the data in Figure 8 as described in Equations 7–12. The reduction and oxidation reaction pathways represented by the small loop in the right hand side of Figure 9 are those occurring in a Li-O_2 battery cell as discussed below.

FePC/KB(300) and FePC/KB(600) catalysts doubled the cycle life of Li-O_2 battery cells compared to those tested without these cathode catalysts. The data are summarized in Figure 11. These Li/O_2 cells

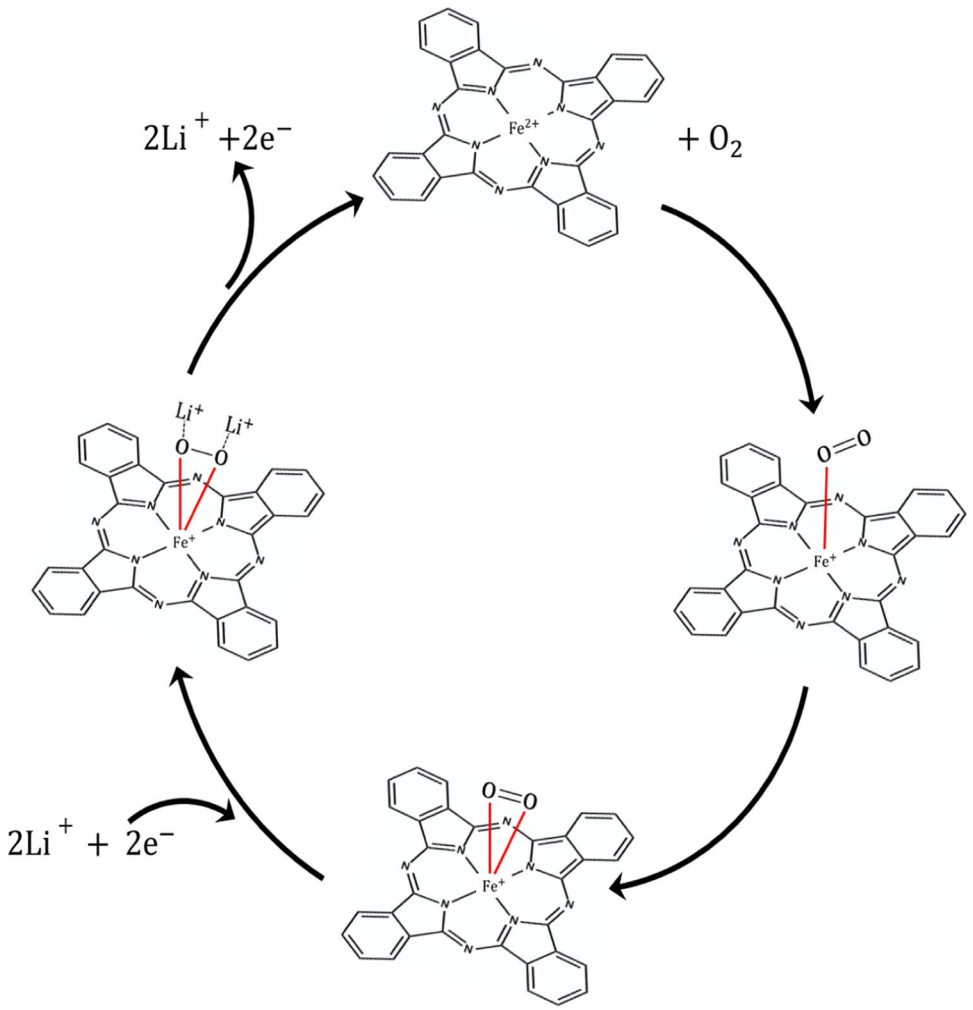

Figure 10. Pathway (ii) - Proposed mechanism of the catalysis of oxygen reduction and oxygen evolution reactions at the FePC/VC(300 and 600) catalysts.

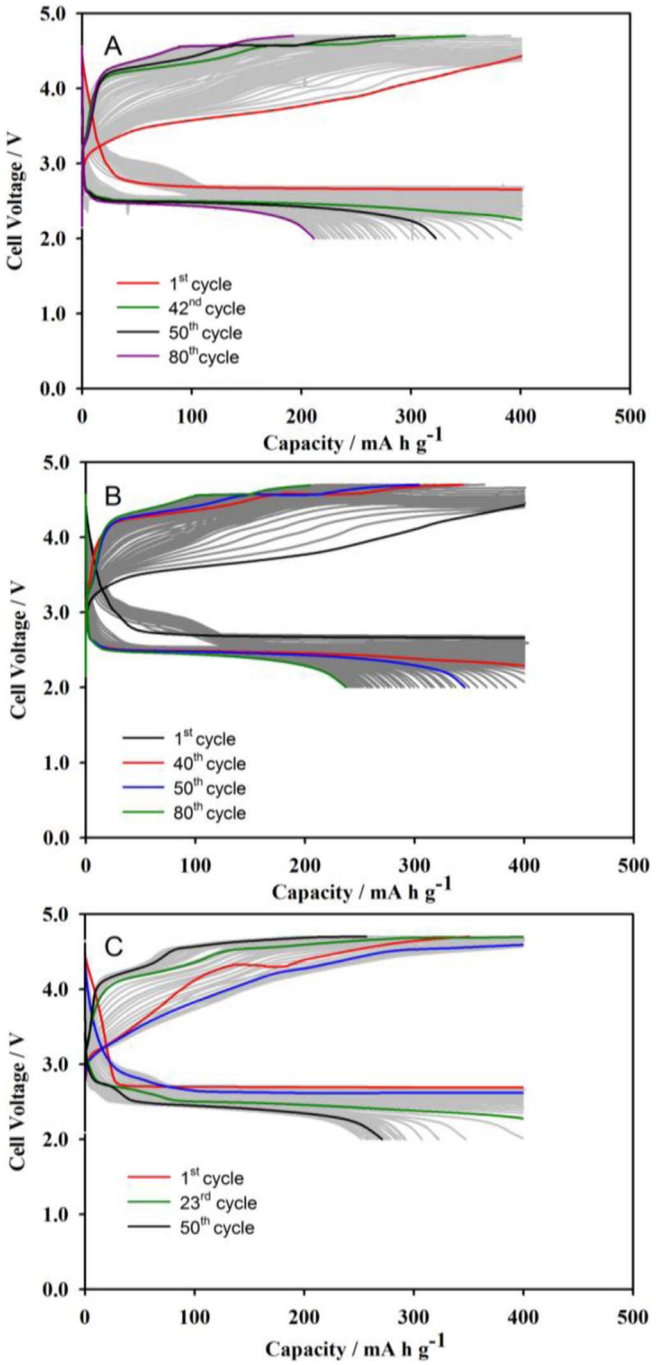

Figure 11. Cycling performance obtained for A) FePC/KB(300) B) FePC/KB(600) C) uncatalyzed(Ketjenblack) cells in 1 M $LiCF_3SO_3$/TEGDME. The cell discharge capacity is limited to 400 mAh/g. The charge limit is 4.65 V.

were cycled with a capacity limit of 400 mAh g^{-1} (Figure 11). The two catalyzed cells with FePC/KB(300) and FePC/KB(600) survived through their 40th cycle with 100% capacity utilization. This is a two-fold increase in cycle life compared to the un-catalyzed Li-O_2 cell (Figure 11C). The other notable feature is the overall lower charge voltage of the catalyzed cells in early cycles which suggest that the catalysts also exert activity for the oxidation (OER) reactions. The oxygen evolution overpotential seems to increase after some early cycles. This is probably caused as mentioned above by (i) degradation of the FePC catalytic sites from reaction with the oxygen reduction reaction intermediate O_2^- and (ii) the insulating lithium oxides poisoning the catalyst.

Catalysis of the oxidation of the O_2 reduction products is not clear in the CV data because of the aforementioned passivation of the electrode at the end of ORR. By limiting the capacity utilization to 400 mAh g^{-1} in the battery cell, the electrodes remain active to catalyze the charge reaction. Interestingly, our XRD and Raman spectral analyses of the products from discharged Li-O_2 cells presented below indicated the presence of both lithium superoxide (LiO_2) and Li_2O_2, providing further support for the discharge reaction mechanisms in these cells utilizing the catalyzed electrodes.

Figure 12 is a comparison of XRD spectra obtained for uncatalyzed and FePC/KB(600) catalyzed Li-O_2 cell cathodes after full discharge with a capacity utilization of 3100 mAh/g (of the Ketjenblack electrode). Weak XRD peaks corresponding to Li_2O_2 are observed initially. Upon standing in the atmosphere for more than 12 hours strong LiOH peaks were observed in the catalyzed cathode. The peaks shown by asterisks are associated with the LiOH formed. The peaks shown by inverted triangles show the Li_2O_2 peak positions. The emergence of the strong LiOH peak upon exposure to humidity indicates that a product besides Li_2O_2 is accumulated on the discharged cathode, possibly lithium superoxide, LiO_2, which is not detectable by XRD. In order to identify LiO_2, a Raman spectrum was recorded on the same cathode before exposing the electrode to the atmosphere (Figure 13). The Raman spectrum of the electrode compared with that for KO_2 indeed shows the presence of LiO_2. The uncatalyzed electrode only shows Li_2O_2 as the discharge product. This further confirms that LiO_2 is produced as the initial discharge product and is stabilized by the Fe(I)-N_4 metal center as Fe(I)-N_4–O_2Li. Some of it is converted to Li_2O_2 via chemical decomposition as shown in Equation 8 and the rest is oxidized to O_2 in the charge half cycle as depicted Equations 14 and 15 and the right hand side loop in Figure 10.

Since the Li-O_2 cells are operated in a continuous flow of O_2 maintaining a constant discharge potential, the one-electron reduction of O_2 to LiO_2 is the predominant discharge reaction. Because the ORR in the Li-O_2 cell is thus confined to the superoxide formation, the differences arising from the different polymorphisms of FePC in the two catalysts do not come into play on the reaction mechanism. On both catalysts the LiO_2 formed initially is converted to Li_2O_2 via the well-established chemical decomposition reaction. However, the stability and life time of the superoxide is determined by the nature of the catalytic site. The Fe/KB(600) appears to provide a longer life time for the adsorbed LiO_2 as the Fe-Fe distance in the catalyst is too long for the efficient chemical conversion of LiO_2 to Li_2O_2. These catalyzed electrodes also catalyze the oxidation of LiO_2 and Li_2O_2 to O_2 at lower voltages in the charge half cycle. The catalysis of both the discharge and charge reactions account for the doubling of the cycle life of the Li-O_2 cell with the catalyzed electrodes. However, the Li_2O_2 formed in each cell by chemical decomposition would passivate the electrode during prolonged cycling and decrease the catalytic activity of the reaction sites. Therefore, long-term operation of catalyzed Li-O_2 cell decreases the activity of the catalyst to affect the cell's cycle life.

Conclusions

Iron(II) phthalocyanine/carbon–based electrode materials prepared by heat-treating FePC embedded in carbon black at 300°C or 600°C have shown evidence for ORR and OER catalysis. In Li^+-containing electrolytes in low DN solvents such as MeCN, the Fe(II)/Fe(I) redox potential appears above the ORR onset potential. As a result the 3d eg^1 electronic configuration of iron in the Fe(I) state is situated at an appropriate potential to stabilize the superoxide ion formed by one-electron reduction of O_2. The ORR takes place at the inner- Helmholtz plane of the catalyzed electrode in these electrolytes. The Fe-Fe interatomic distance in α-FePC favors interaction of the O_2 residing on adjacent Fe(I) centers leading to efficient conversion of the superoxide to peroxide by chemical decomposition. The peroxide formed is in turn reduced to lithium monoxide at

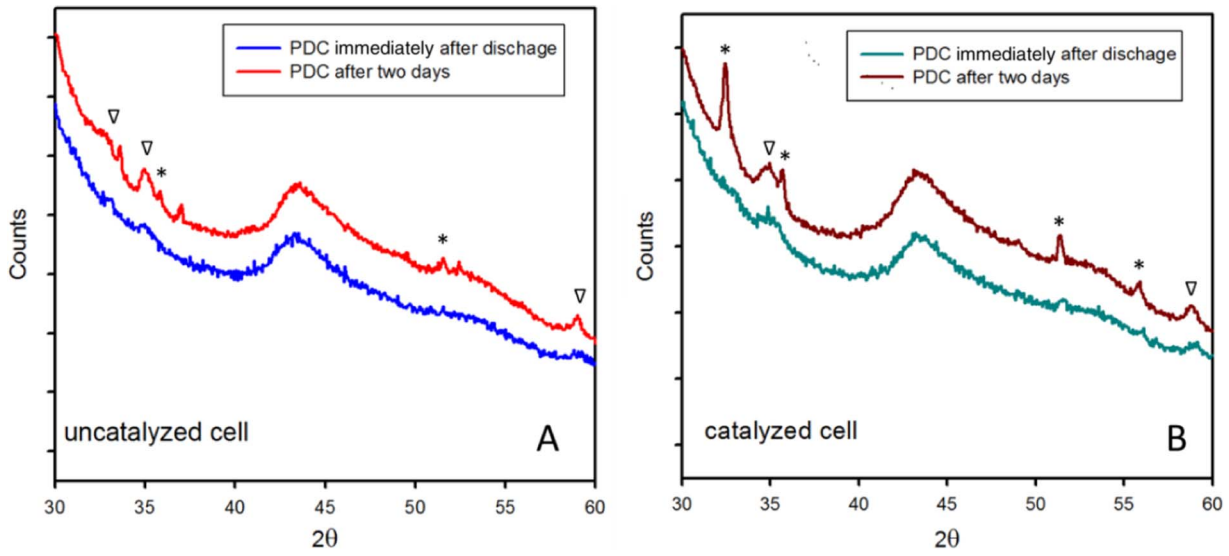

Figure 12. XRD profile for the post discharged cathodes. A) Post-Discharge-Cathode using KB300JD, B) Post-Discharge-Cathode using FePC/KB(600)(uncatalyzed). Peaks marked inverted triangles are due to Li_2O_2 and the asterisks are associated with LiOH.

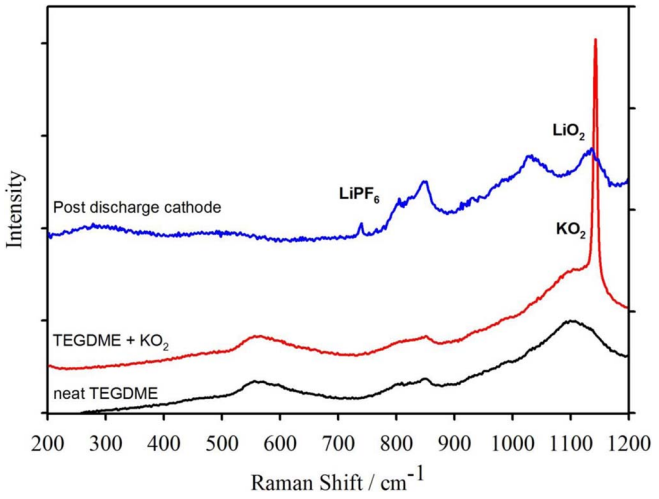

Figure 13. Raman Spectrum obtained for the post discharge cathode (FePC/KB(600)). The red and black curves show the spectra obtained for the TEGDME solvent + K_2O powder and neat TEGDME respectively.

the FePC/VC(300) electrode polarized to lower potentials. In high DN dimethyl sulfoxide-based electrolytes LiO_2 is more stable in its solvated state as the $Li(DMSO)_n$–O_2^- ion pair specie. This drives the ORR on catalyzed electrodes in DMSO at the outer-Helmholtz plane. Our data suggest that the presence of the Fe(I)-N_4 center is essential for catalytic O_2 reduction reaction. The FePC/carbon–based catalysts can be employed in Li-O_2 batteries to catalyze both ORR and OER leading to longer cycle life for the battery.

Acknowledgment

Financial support from US Army Cerdec via subcontract No: GTS-S-15-015 is gratefully acknowledged.

References

1. K. M. Abraham, *Journal of The Electrochemical Society*, **162**(2), A3021 (2015).
2. M. J. Trahan, I. Gunasekara, S. Mukerjee, E. J. Plichta, M. A. Hendrickson, and K. M. Abraham, *Journal of The Electrochemical Society*, **161**(10), A1706 (2014).
3. M. J. Trahan, Q. Jia, S. Mukerjee, E. J. Plichta, M. A. Hendrickson, and K. M. Abraham, *Journal of The Electrochemical Society*, **160**(9), A1577 (2013).
4. Y.-C. Lu and Y. Shao-Horn, *The Journal of Physical Chemistry Letters*, **4**(1), 93 (2013).
5. Y. Shao, S. Park, J. Xiao, J.-G. Zhang, Y. Wang, and J. Liu, *ACS Catalysis*, **2**(5), 844 (2012).
6. K. M. Abraham and Z. Jiang, *Journal of The Electrochemical Society*, **143**(1), 1 (1996).
7. C. Fierro, A. B. Anderson, and D. A. Scherson, *The Journal of Physical Chemistry*, **92**(24), 6902 (1988).
8. J.-L. Shui, N. K. Karan, M. Balasubramanian, S.-Y. Li, and D.-J. Liu, *Journal of the American Chemical Society*, **134**(40), 16654 (2012).
9. C. W. B. Bezerra, L. Zhang, K. Lee, H. Liu, A. L. B. Marques, E. P. Marques, H. Wang, and J. Zhang, *Electrochimica Acta*, **53**(15), 4937 (2008).
10. A. B. P. Lever and P. C. Minor, *Advances in Molecular Relaxation and Interaction Processes*, **18**(2), 115 (1980).
11. D. Sun, Y. Shen, W. Zhang, L. Yu, Z. Yi, W. Yin, D. Wang, Y. Huang, J. Wang, D. Wang, and J. B. Goodenough, *Journal of the American Chemical Society*, **136**(25), 8941 (2014).
12. A. J. Wain, G. G. Wildgoose, C. G. R. Heald, L. Jiang, T. G. J. Jones, and R. G. Compton, *The Journal of Physical Chemistry B*, **109**(9), 3971 (2005).
13. M. Ladouceur, G. Lalande, D. Guay, J. Dodelet, L. Dignard-Bailey, M. Trudeau, and R. Schulz, *Journal of the Electrochemical Society*, **140**(7), 1974 (1993).
14. M. J. Trahan, S. Mukerjee, E. J. Plichta, M. A. Hendrickson, and K. M. Abraham, *Journal of The Electrochemical Society*, **160**(2), A259 (2013).
15. K. Kadish, R. Guilard, and K. M. Smith, *The Porphyrin Handbook: Phthalocyanines: spectroscopic and electrochemical characterization*. Academic press: 2003; Vol. **16**.
16. J. G. Jones and M. V. Twigg, *Inorganic Chemistry*, **8**(10), 2120 (1969).
17. E. Milaeva, G. Speier, and A. Lever *The redox chemistry of metallophthalocyanines in solution*; DTIC Document: 1992.
18. I. Gunasekara, S. Mukerjee, and K. M. Abraham In *Microelectrode Investigations of Oxygen Reduction Reactions in Lithium-Air Batteries*, ECS Meeting Abstracts, ECS Meeting Abstracts, October 27, 2013; ECS Meeting Abstracts, 2013; p 449.
19. W. Linert, A. Camard, M. Armand, and C. Michot, *Coordination Chemistry Reviews*, **226**(1–2), 137 (2002).
20. A. S. Milev, N. Tran, G. S. Kamali Kannangara, M. A. Wilson, and I. Avramov, *The Journal of Physical Chemistry C*, **112**(14), 5339 (2008).
21. V. Bambagioni, C. Bianchini, J. Filippi, A. Lavacchi, W. Oberhauser, A. Marchionni, S. Moneti, F. Vizza, R. Psaro, V. Dal Santo, A. Gallo, S. Recchia, and L. Sordelli, *Journal of Power Sources*, **196**(5), 2519 (2011).
22. C. Melendres and V. Maroni, *Journal of Raman spectroscopy*, **15**(5), 319 (1984).
23. J. Janczak and R. Kubiak, *Inorganica Chimica Acta*, **342**(0), 64 (2003).
24. C. O. Laoire, S. Mukerjee, K. M. Abraham, E. J. Plichta, and M. A. Hendrickson, *The Journal of Physical Chemistry C*, **114**(19), 9178 (2010).
25. C. O. Laoire, S. Mukerjee, K. M. Abraham, E. J. Plichta, and M. A. Hendrickson, *The Journal of Physical Chemistry C*, **113**(46), 20127 (2009).